Journal of Pharmaceutical Analysis 14 (2024) 100902

Contents lists available at ScienceDirect

Journal of Pharmaceutical Analysis

journal homepage: www.elsevier.com/locate/jpa

Original article

Ginsenoside Rb1 induces hepatic stellate cell ferroptosis to alleviate liver fibrosis via the BECN1/SLC7A11 axis

Lifan Lin [a], Xinmiao Li [a], Yifei Li [a], Zhichao Lang [a], Yeping Li [b, **], Jianjian Zheng [c, *]

[a] Key Laboratory of Diagnosis and Treatment of Severe Hepato-Pancreatic Diseases of Zhejiang Province, The First Affiliated Hospital of Wenzhou Medical University, Wenzhou, Zhejiang, 325000, China
[b] Department of Urology, The First Affiliated Hospital of Wenzhou Medical University, Wenzhou, Zhejiang, 325000, China
[c] Key Laboratory of Clinical Laboratory Diagnosis and Translational Research of Zhejiang Province, The First Affiliated Hospital of Wenzhou Medical University, Wenzhou, Zhejiang, 325000, China

ARTICLE INFO

Article history:
Received 29 August 2023
Received in revised form
2 November 2023
Accepted 21 November 2023
Available online 29 November 2023

Keywords:
Ginsenoside Rb1
Ferroptosis
Liver fibrosis
Hepatic stellate cells

ABSTRACT

Liver fibrosis is primarily driven by the activation of hepatic stellate cells (HSCs), a process associated with ferroptosis. Ginsenoside Rb1 (GRb1), a major active component extracted from Panax ginseng, inhibits HSC activation. However, the potential role of GRb1 in mediating HSC ferroptosis remains unclear. This study examined the effect of GRb1 on liver fibrosis both *in vivo* and *in vitro*, using CCl_4-induced liver fibrosis mouse model and primary HSCs, LX-2 cells. The findings revealed that GRb1 effectively inactivated HSCs *in vitro*, reducing alpha-smooth muscle actin (α-SMA) and Type I collagen (Col1A1) levels. Moreover, GRb1 significantly alleviated CCl_4-induced liver fibrosis *in vivo*. From a mechanistic standpoint, the ferroptosis pathway appeared to be central to the antifibrotic effects of GRb1. Specifically, GRb1 promoted HSC ferroptosis both *in vivo* and *in vitro*, characterized by increased glutathione depletion, malondialdehyde production, iron overload, and accumulation of reactive oxygen species (ROS). Intriguingly, GRb1 increased Beclin 1 (BECN1) levels and decreased the System Xc-key subunit SLC7A11. Further experiments showed that BECN1 silencing inhibited GRb1-induced effects on HSC ferroptosis and mitigated the reduction of SLC7A11 caused by GRb1. Moreover, BECN1 could directly interact with SLC7A11, initiating HSC ferroptosis. In conclusion, the suppression of BECN1 counteracted the effects of GRb1 on HSC inactivation both *in vivo* and *in vitro*. Overall, this study highlights the novel role of GRb1 in inducing HSC ferroptosis and promoting HSC inactivation, at least partly through its modulation of BECN1 and SLC7A11.

1. Introduction

Liver fibrosis is a complex physiological response to chronic liver injury, characterized by an excessive accumulation of extracellular matrix (ECM) and the activation of hepatic stellate cells (HSCs) [1]. During liver fibrosis, normal liver structures are replaced with numerous fibrous nodules and pseudolobules, leading to liver dysfunction [2]. Without effective treatment, this dysfunction can progress to cirrhosis and may subsequently trigger the onset of hepatocellular carcinoma (HCC) [3]. Activated HSCs serve as the primary source of ECM [4]. Thus, strategies focused on inducing HSC inactivation present therapeutic potential for combating liver fibrosis.

Ferroptosis is a recently identified form of programmed cell death, characterized by the accumulation of reactive oxygen species (ROS) and an excess of iron [5,6]. Ferroptosis is linked with alterations in mitochondrial morphology, such as reduced volume, increased membrane density, and lack of cristae [7]. The relationship between the development of cancer and ferroptosis has also been documented [8]. Moreover, emerging evidence suggests a role for ferroptosis in liver fibrosis development. For example, Luo et al. [9] reported that celastrol mitigates hepatic fibrosis by inducing ferroptosis in HSCs. However, the relationship between ferroptosis and HSC activation requires more extensive research.

Chinese herbal medicines such as isoliquiritigenin, phloretin, and Radix Paeoniae Alba have shown potential to mitigate disease progression or processes such as liver fibrosis, pancreatic cancer, and inflammation [10–12]. Panax ginseng, a traditional herbal medicine, is widely used to treat various human diseases [13]. Ginsenoside Rb1 (GRb1), a key active component of Panax ginseng, possesses anti-inflammatory, anti-oxidative, and anti-fibrotic properties [14]. For instance, Ni et al. [15] revealed that GRb1 ameliorates renal fibrosis by targeting the Bip/eIF2α/CHOP axis-

* Corresponding author.
** Corresponding author.
E-mail addresses: zjj@wmu.edu.cn (J. Zheng), liypwz@126.com (Y. Li).

https://doi.org/10.1016/j.jpha.2023.11.009

mediated epithelial-mesenchymal transition. Nonetheless, the specific mechanisms through which GRb1 counters liver fibrosis remain largely unexplored. Thus, this study aimed to discern the potential role of HSC ferroptosis in mediating the therapeutic effects of GRb1 on liver fibrosis.

2. Materials and methods

2.1. Materials

Primary antibodies against alpha-smooth muscle actin (α-SMA; ab124964), Type I collagen (Col1A1; ab254113 and ab138492), β-actin (ab6276), Beclin 1 (BECN1; ab207612), and SLC7A11 (ab175186) were obtained from Abcam (Shanghai, China). GRb1 (≥95% purity; Y0001347), CCl_4 (488488), curcumin (Cur; C1386), ferrostatin-1 (Fer-1; SML0583), Z-VAD-FMK (219007), necrostatin-1 (Nec-1; 480065), and erastin (Era; 329600) were purchased from Sigma-Aldrich (St. Louis, MO, USA). The chemical structure of GRb1 is shown in Fig. 1A.

2.2. Animal experiments

Male C57BL/6J mice (6–8 weeks old, weighing 18–22 g) were obtained from Zhejiang Weitong Lihua Experimental Animal

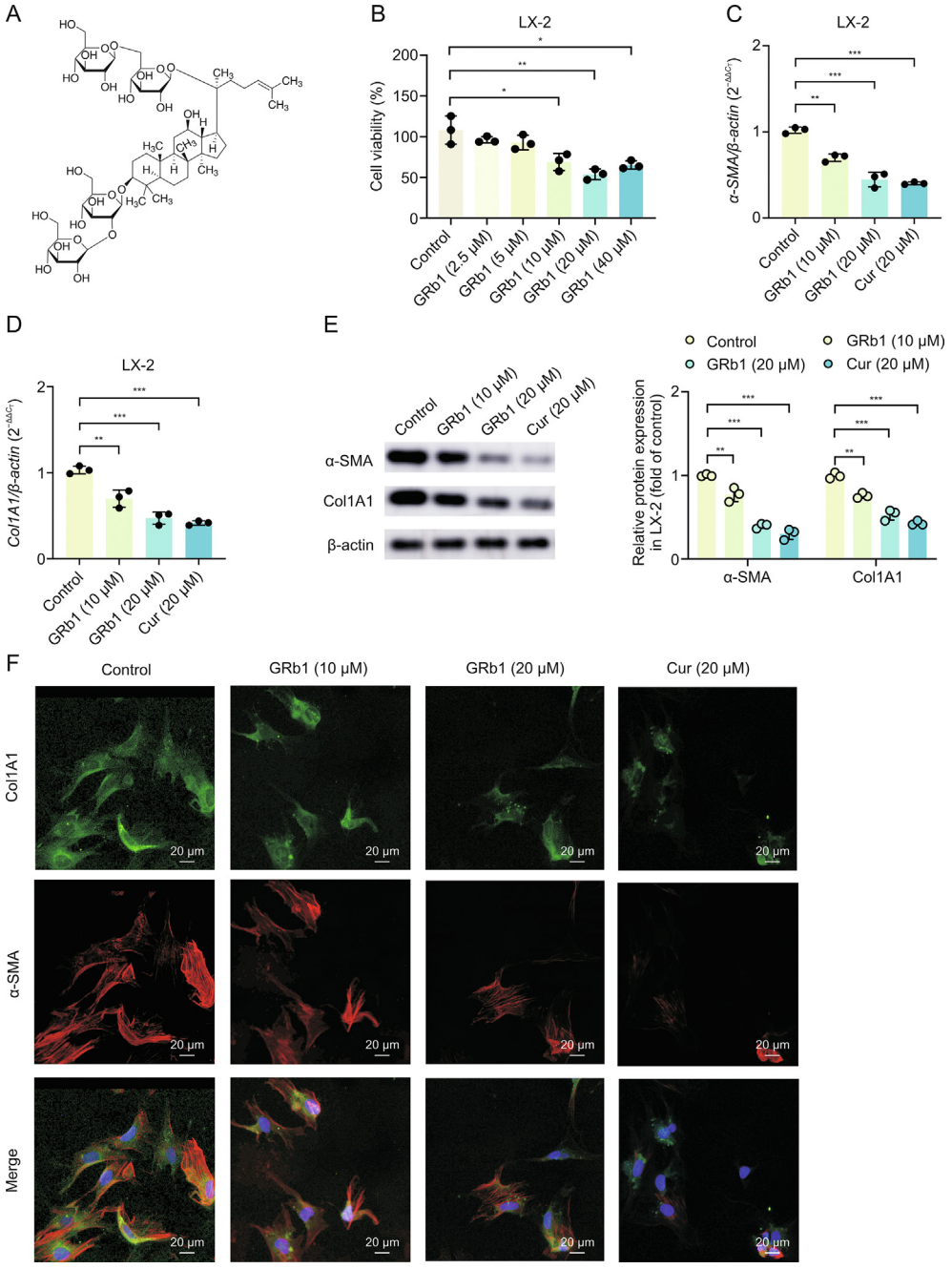

Fig. 1. Ginsenoside Rb1 (GRb1) suppresses hepatic stellate cell (HSC) activation in LX-2 cells. LX-2 cells were treated with varying concentrations of GRb1 (0, 2.5, 5, 10, 20, and 40 μM) over 24 h. (A) Representation of GRb1's chemical structure. (B) Cell viability post GRb1 treatment. (C, D) Messenger RNA (mRNA) expression levels of alpha-smooth muscle actin (*α-SMA*) (C) and type I collagen (*Col1A1*) (D). (E) Protein expression levels of α-SMA and Col1A1. (F) Co-localization of α-SMA (shown in red) and Col1A1 (shown in green) in LX-2 cells was analyzed using immunofluorescence staining. 4′,6-diamidino-2-phenylindole (DAPI) was used to stain nuclei in blue. $^{*}P < 0.05$, $^{**}P < 0.01$, and $^{***}P < 0.001$. Cur: curcumin.

Technology Co., Ltd. (Jiaxing, China). An intraperitoneal injection of CCl_4 in olive oil (10%, 7 μL/g) was performed to induce hepatic fibrosis in mice [16]. The mice were then randomly segregated into either five or four groups ($n = 6$ per group). To ascertain GRb1's impact, mice in groups 1–5 received the subsequent treatments: group 1, olive oil; group 2, CCl_4; group 3, 10 mg/kg GRb1; group 4, 20 mg/kg GRb1; and group 5, 200 mg/kg Cur. Mice in groups 2–5 received intraperitoneal injections of CCl_4 twice a week for eight weeks. During this period, GRb1 in phosphate-buffered saline (PBS) was administered daily through gavage, while Cur was administered every alternate day. In another set, mice from four groups received treatments of olive oil, i.e., CCl_4 + vitamin A-coupled liposomes (VA-Lip)-control-vector, CCl_4 + VA-Lip-control-vector + GRb1, or CCl_4 + VA-Lip-BECN1-short hairpin RNA (shRNA) + GRb1. The mice also received intraperitoneal injections of CCl_4 in olive oil twice weekly for eight weeks. Controls received an equivalent amount of olive oil. The 20 mg/kg GRb1 in PBS was fed daily through gavage during CCl_4 injection. After the CCl_4 injection, VA-Lip-control-vector and VA-Lip-BECN1-shRNA (0.75 mg/kg) were intravenously delivered thrice weekly over two weeks. All animal experiments received approval from the Experimental Animal Center of Wenzhou Medical University, China (Approval No.: wydw2023–0146).

2.3. Pathological examination and immunohistochemistry

After deparaffinization and rehydration, paraffin liver sections (4-μm thick) were stained using Masson's and Sirius red stain (ab150669 and ab150681; Abcam). For immunohistochemical staining, liver tissue sections were permeabilized, blocked, and then incubated with the primary antibody against α-SMA overnight at 4 °C. Subsequently, sections were incubated with a horseradish peroxidase-labeled secondary antibody (Abcam) at room temperature for 1 h. Nuclei were stained using hematoxylin. Images captured through a microscope (Leica Microsystems, Wetzlar, Germany) were analyzed using ImageJ software.

2.4. Isolation of primary HSCs

Primary HSCs were extracted from the mouse liver as previously described [17]. In brief, mice livers were subjected to perfusion through the portal vein *in situ*, sequentially with Ca^{2+}-free Hanks' Balanced Salt Solution (HBSS) (Thermo Fisher Scientific Inc., Waltham, MA, USA) for 15 min, 100 mL of 0.2% pronase solution, and then with 0.2% collagenase type IV (Sigma-Aldrich). The resulting cell suspension was filtered through a 100-μm pore mesh-sized nylon filter and centrifuged at 200 *g* for 10 min. The supernatant was collected for the isolation of primary HSCs. Commercially available 11.5% Percoll (Sigma-Aldrich) was prepared, and the supernatant was added to the upper layer of Percoll carefully, after which the contents were centrifuged at 450 *g* for 10 min. The sediment was then resuspended in 0.5 mL of HBSS and centrifuged at 1,400 *g* for 25 min. Finally, primary HSCs were harvested from the upper layer of the Optiprep solution.

2.5. Cell culture and dosing treatment

LX-2 cells were sourced from Procell Life Science & Technology Co., Ltd. (Wuhan, China). Both primary HSCs and LX-2 cells were cultured in Dulbecco's modified Eagle's medium (DMEM) supplemented with 10% (*V*/*V*) fetal bovine serum (FBS; Gibco, Grand Island, NY, USA) and 1% penicillin/streptomycin (Gibco). LX-2 cells and primary HSCs were treated with GRb1 (10 or 20 μM), Era (10 μM), and Fer-1 (1 μM) for 24 h. Additionally, LX-2 cells were treated with Cur (20 μM) for 24 h. Cells undergoing GRb1 treatment also received Fer-1 (1 μM), Nec-1 (10 μM), and Z-VAD-FMK (10 μM) for the same duration. Control cells were cultured in a medium devoid of drugs, containing equivalent amounts of dimethyl sulfoxide (DMSO).

2.6. Detection of biochemical parameters

The levels of alanine aminotransferase (ALT), aspartate transaminase (AST), hyaluronic acid (HA), laminin (LN), procollagen type III (PC-III), and collagen type IV (IV-C) were assessed using commercial kits (Jiancheng Bioengineering Institute, Nanjing, China) according to the manufacturer's instructions.

2.7. Cell Counting Kit-8 (CCK-8) assay

Cell viability was determined by seeding 7×10^3 cells in 96-well plates and exposing them to different drug concentrations for 24 h. Subsequently, 10 μL of CCK-8 (C0038; Beyotime, Shanghai, China) was added to each well, followed by a 30 min incubation at 37 °C. Optical densities were then recorded at 450 nm.

2.8. 5-Ethynyl-2′-deoxyuridine (EdU) assay

To evaluate HSC proliferation, an EdU cell proliferation kit (C0078S; Beyotime) was used. After EdU labeling for 48 h, primary HSC and LX-2 cells were fixed in formalin and permeabilized with 0.3% Triton X-100. Cells were subsequently incubated with Apollo567 staining reaction solution in the dark for 30 min. The viable cells were counted post-staining.

2.9. Iron assay

Iron content was quantified using an iron assay kit (ab83366; Abcam) as previously described [18]. In essence, the iron assay buffer releases ferric ions from ferric carrier proteins, allowing for the measurement of total iron concentration. Insoluble materials were removed by centrifugation at 13,000 *g* for 15 min at 4 °C, and optical densities were read at 593 nm.

2.10. Lipid ROS assay

Lipid ROS levels were assessed using the C11-BODIPY probe (ajci64572; Amgicam, Wuhan, China), following the manufacturer's instructions. Briefly, cells were treated with 1 mL of C11-BODIPY and washed twice after a 60 min incubation at 37 °C. Cells were subsequently resuspended in 500 μL of PBS, and lipid ROS levels were quantified using the FACS Calibur Flow Cytometer (BD Biosciences, San Jose, CA, USA).

2.11. Malondialdehyde (MDA) assay

MDA levels were determined using a lipid peroxidation assay kit (ab118970; Abcam). Specifically, cell lysate supernatants were gathered, and 600 μL of thiobarbituric acid solution was added to every well. The samples were incubated. After incubation at 95 °C for 60 min and cooling to room temperature in an ice bath for 10 min, 200 μL of the reaction mixture was transferred to a 96-well plate. MDA content was then measured at 532 nm using a microplate reader (Thermo Fisher Scientific Inc.).

2.12. Glutathione (GSH) assay

The GSH levels were measured using a GSH assay kit (CS0260; Sigma-Aldrich). Cells were washed with cold PBS and treated with 5% 5-sulfosalicylic acid solution, and samples were centrifuged at

10,000 *g* for 10 min. Then, 150 μL of GSH working mixture was added to each sample, incubated at room temperature for 5 min, followed by treatment with 50 μL of diluted nicotinamide adenine dinucleotide phosphate (NADPH) solution. The resulting yellow product was quantified at 412 nm using a microplate reader (Thermo Fisher Scientific Inc.).

2.13. Transmission electron microscopy (TEM)

Briefly, for TEM analysis, cells were fixed using an electron microscope fixing solution for 2–4 h, embedded in 1% agarose, dehydrated, and sectioned into ultrathin slices (60–80 nm thickness) using an ultramicrotome (Leica Microsystems). Sections were then stained with 2% ethanol-saturated uranyl acetate and lead citrate solution for 15 min and allowed to dry overnight at room temperature. Images were captured using a transmission electron microscope.

2.14. Quantitative real-time reverse transcription-polymerase chain reaction (qRT-PCR)

Total RNA from liver tissues or cells was extracted with TRIzol reagents (15596026; Thermo Fisher Scientific Inc.). Complementary DNA (cDNA) was synthesized using a reverse transcription kit (A3500; Promega, Beijing, China). The SYBR Green Master Mix (TOROIVD, Shanghai, China) was employed to determine gene expression levels, referencing β-actin. The related primer sequences are provided in Table S1.

2.15. Western blot

Proteins were extracted from liver tissues and cells using radioimmunoprecipitation assay (RIPA) lysis buffer, and their concentrations were determined using a bicinchoninic acid (BCA) kit (P0011; Beyotime). The proteins were then separated using 10% sodium dodecyl sulfate-polyacrylamide gel electrophoresis (SDS-PAGE) and transferred onto polyvinylidene difluoride (PVDF) membranes (Thermo Fisher Scientific Inc.). After blocking, membranes were incubated with primary antibodies, including anti-α-SMA, anti-Col1A1, anti-SLC7A11, anti-BECN1, and anti-β-actin (used as an internal control), overnight at 4 °C. Membranes were subsequently exposed to secondary antibodies for 1 h at room temperature. Protein expression was quantified using ImageJ software.

2.16. Immunofluorescence assay

After immobilizing with 4% (*V*/*V*) paraformaldehyde (P0099; Beyotime) and a PBS wash, primary HSCs and LX-2 cells were permeabilized using 0.5% (*V*/*V*) Triton X-100 and blocked with 5% (*V*/*V*) bovine serum albumin (BSA) for 30 min. They were then treated with primary antibodies, including anti-α-SMA (ab124964), anti-Col1A1 (ab283694), anti-BECN1 (ab62557), and anti-SLC7A11 (ab307601). After this, cells were stained with secondary antibodies, and nuclei were stained with 4′,6-diamidino-2-phenylindole (DAPI) (C1005; Beyotime). The prepared samples were visualized under a microscope (Nikon, Tokyo, Japan).

2.17. Co-immunoprecipitation (Co-IP)

Cells were lysed at 4 °C in lysis buffer supplemented with protease inhibitors, followed by transient centrifugation. After incubating the samples with either IgG or specific antibodies overnight at 4 °C, they were combined with magnetic beads (Thermo Fisher Scientific Inc.) for 2 h at 4 °C. The precipitate was then washed with lysate. Proteins were eluted by boiling in a sample buffer for subsequent Western blot analysis.

2.18. Molecular docking analysis

The crystal structures of BECN1 (AF-O88597-F1) and SLC7A11 (PDB ID: 7p9u) were sourced from the AlphaFold database and Protein Data Bank (PDB) respectively. Before molecular docking, the proteins underwent preparations, including molecular energy minimization, removal of water molecules, and the addition of hydrogen atoms using PyMOL. Molecular docking was then executed using molecular orbital environment (MOE, 2015) software. Results from the protein-protein DOCK module of MOE were visualized using PyMOL software.

2.19. RNA interference and overexpression

Primary HSCs and LX-2 cells underwent transfection with BECN1 small interfering RNA (siRNA) or a scrambled (negative) control (control siRNA) (GenePharma Co., Ltd., Shanghai, China) using Lipofectamine™ 3000 (Invitrogen, Carlsbad, CA, USA) for 24 h. For BECN1 overexpression, cells were transfected with BECN1 overexpression plasmid (BECN cDNA) or an empty plasmid (control cDNA) using Lipofectamine™ 3000 for 24 h. After transfection, cells received a 20 μM GRb1 treatment for 24 h.

2.20. Virus construction

VA-Lip-BECN1-shRNA was constructed as previously described [19]. In brief, a VA solution was produced by mixing 50 μL of DMSO with 5 mg of VA. A combined solution of LipoTrust (0.14 μmol) and VA (280 nmol) was then prepared in a tube (AM12450; Thermo Fisher Scientific Inc.) at 25 °C. This VA-Lip solution was combined with BECN1-shRNA and a control vector (Santa Cruz Biotechnology, Shanghai, China) while stirring continuously. The resultant material was filtered by filter (596-3320; Thermo Fisher Scientific Inc.), and the collected fractions were used for subsequent *in vivo* applications.

2.21. RNA sequencing (RNA-seq)

Total RNA extraction was conducted using the TRIzol reagent (15596026; Thermo Fisher Scientific Inc.). Briefly, RNA-seq libraries were created using the KAPA Stranded RNA-Seq Library Prep Kit (Illumina, San Diego, CA, USA). Library quality was evaluated with the Agilent 2100 Bioanalyzer (Agilent Technologies, Santa Clara, CA, USA), and library quantification was performed through qRT-PCR. The Illumina NovaSeq 6000 sequencer was used to sequence diverse libraries. Transcripts with expressions showcasing $|\log2(\text{fold change})| > 2$ and an adjusted P-value < 0.05 were deemed to be statistically significant.

2.22. Statistical analysis

All experimental procedures were replicated three times (*in vitro*) and six times (*in vivo*). The results were displayed as the mean ± standard deviation. Data analysis was executed using 17.0 SPSS software (SPSS, Chicago, IL, USA). Multiple groups were compared using a one-way analysis of variance (ANOVA), while the Student's *t*-test was employed for comparisons between two groups. A P-value of <0.05 was considered to be statistically significant.

3. Results

3.1. GRb1 impedes the activation of HSC in vitro

Prior research has indicated that GRb1 can inhibit HSC activation [20]. To delve deeper into GRb1's potential to promote HSC inactivation, the proliferation rate was evaluated and activation markers (α-SMA and Col1A1) were observed in LX-2 cells treated with GRb1. Notably, GRb1 reduced HSC proliferation, with a striking effect at 20 μM, recording a 47% reduction (Fig. 1B). Based on this outcome, 10 and 20 μM GRb1 concentrations were selected for all ensuing experiments. GRb1 treatment significantly lowered the levels of α-SMA and Col1A1 compared with the control group (Fig. 1C–E). In line with these results, immunofluorescence assessments further highlighted a decrease in α-SMA and Col1A1 levels in HSCs due to GRb1 (Fig. 1F). Moreover, the positive control, Cur, similarly triggered HSC inactivation (Figs. 1C–F). Taken together, these findings advocate that GRb1 facilitates HSC inactivation.

3.2. GRb1 alleviates liver fibrosis through HSC ferroptosis in vivo

To investigate the potential of GRb1 in suppressing liver fibrosis *in vivo*, fibrosis-related markers were analyzed in CCl_4-induced mice administered with GRb1. The data showed a pronounced increase in HA, LN, PC-III, and IV-C levels in the CCl_4-treated mice, an effect attenuated upon GRb1 or Cur treatment (Figs. S1A–D). Additionally, collagen accumulation in CCl_4-induced mice post-GRb1 treatment was evaluated using Masson and Sirius Red stains. The results revealed a significant reduction in collagen accumulation in both GRb1 and Cur-treated groups compared with the CCl_4-only group (Fig. 2A). Echoing these findings, post-CCl_4 treatment, messenger RNA (mRNA) levels of HSC activation markers, specifically α-SMA and Col1A1, surged to 398% and 438% respectively. Introducing 10 mg/kg GRb1, 20 mg/kg GRb1, and 200 mg/kg Cur resulted in decreased *α-SMA* mRNA levels to 318%, 201%, and 200%, respectively, and reduced *Col1A1* mRNA levels to 338%, 251%, and 251% respectively (Fig. S1E). Additionally, GRb1 markedly countered the elevated ALT and AST levels induced by CCl_4 (Figs. S1F and G).

To understand the mechanisms behind GRb1's antifibrotic effects on liver fibrosis, RNA-seq was performed on liver tissues from CCl_4-treated mice that had received GRb1. Compared with the CCl_4 group, GRb1 administration resulted in a marked decrease in *Slc7a11* expression and a significant elevation in *Becn1* expression (Fig. 2B). qRT-PCR results further confirmed that *Slc7a11* mRNA levels downregulated to 85% and 42%, while *Becn1* mRNA levels upregulated to 263% and 303% in the 10 and 20 mg/kg GRb1 groups, respectively (Fig. 2C). Enrichment analysis highlighted a significant concentration of differentially expressed genes (DEGs) in the ferroptosis pathway (Fig. 2D). Based on this finding, this study hypothesized that GRb1's influence on liver fibrosis might be related to the ferroptosis pathway.

Given the association between GRb1's inhibitory function and the ferroptosis pathway (Fig. 2D) and the evidence that GRb1 can enhance HSC inactivation (Fig. 1), GRb1 was speculated to drive HSC inactivation through HSC ferroptosis. To test this, this study analyzed primary HSCs derived from CCl_4-treated mice that had been treated with either GRb1 or Cur. Additionally, ferroptosis-associated indicators such as GSH, MDA, iron levels, and ROS were assessed. The results indicated a decrease in GSH levels and an increase in MDA, iron, and ROS in the GRb1 + CCl_4 group when compared with the CCl_4-only group (Figs. 2E–H). This underscores the role of ferroptosis in GRb1's action against liver fibrosis. Cur, as a positive drug, contributed to promoting HSC ferroptosis (Figs. 2E–H). Furthermore, this study determined whether GRb1-induced ferroptosis occurred in hepatocytes, liver sinusoidal endothelial cells (LSECs), and macrophages. Yet, no significant variations in ferroptosis markers were detected in primary hepatocytes, LSECs, or macrophages (Fig. S1H). In summary, these findings confirm that GRb1 combats liver fibrosis by inducing HSC ferroptosis *in vivo*.

3.3. GRb1 promotes HSC ferroptosis in vitro

To determine whether GRb1 promotes HSC ferroptosis *in vitro*, this study analyzed HSC proliferation in LX-2 cells and primary HSCs after GRb1 administration. EdU analysis revealed diminished cell proliferation with GRb1 treatment (Figs. 3A and B). Similarly, the CCK-8 assay showed that, relative to untreated cells, cell viability was reduced to 79% and 49% in 10 and 20 μM GRb1-treated LX-2 cells, respectively, and to 77% and 49% in 10 and 20 μM GRb1-treated primary HSCs, respectively (Fig. 3C). Importantly, GRb1 administration led to a significant increase in GSH depletion, MDA production, iron accumulation, and lipid ROS accumulation (Figs. 3D–G). Interestingly, the effects of GRb1 on HSC proliferation and ferroptosis mirrored those of Era (a known ferroptosis inducer; Figs. 3A–G). Moreover, TEM analysis highlighted mitochondrial morphological alterations, including contraction and either reduced or disappeared cristae, in GRb1-treated cells in comparison to the control group (Figs. 3H and I). Overall, these data imply that GRb1 plays a role in boosting HSC ferroptosis *in vitro*.

3.4. GRb1 suppresses HSC activation via ferroptosis

To further corroborate the significance of ferroptosis in GRb1-driven HSC deactivation, this study evaluated the influence of ferroptosis inhibitors on the HSC proliferation induced by GRb1. Significantly, the decline in HSC proliferation triggered by GRb1 was reversed by Fer-1 (a ferroptosis inhibitor), while neither the necroptosis inhibitor (Nec-1) nor the apoptosis inhibitor (Z-VAD-FMK) made any discernible differences (Fig. S2). This evidence reaffirms the role of ferroptosis in the HSC inactivation mediated by GRb1. The GRb1-induced decrease in HSC proliferation and the escalation in GSH depletions, MDA, iron, and ROS were reversed by Fer-1 (Figs. 4A–E). Additionally, the suppression of *α-SMA* and *Col1A1* mRNA levels by GRb1 was negated with Fer-1 intervention (Figs. 4F–I). In conclusion, these results establish that the HSC ferroptosis induced by GRb1 facilitates the suppression of HSC activation.

3.5. GRb1 induces HSC ferroptosis via BECN1

Considering the enrichment of DEGs in the autophagy pathway in GRb1-treated mice (Fig. 2D), this study delved into the role of the autophagy-associated gene *Becn1* in the HSC ferroptosis mediated by GRb1. Notably, *Becn1* is recognized as a pivotal regulator of cancer cell ferroptosis [21]. Its expression exhibited a marked upregulation in the liver tissues of CCl_4-treated mice that were administered GRb1 (Figs. 2B and C). Subsequently, the concentrations of BECN1 and ferroptosis-linked markers, such as SLC7A11, GPX4, ACSL4, and PTGS2, were measured in cells treated with GRb1. Compared with the control, *BECN1* levels surged to 355% in LX-2 cells and 346% in primary HSCs. Meanwhile, *SLC7A11* levels decreased to 40% in LX-2 cells

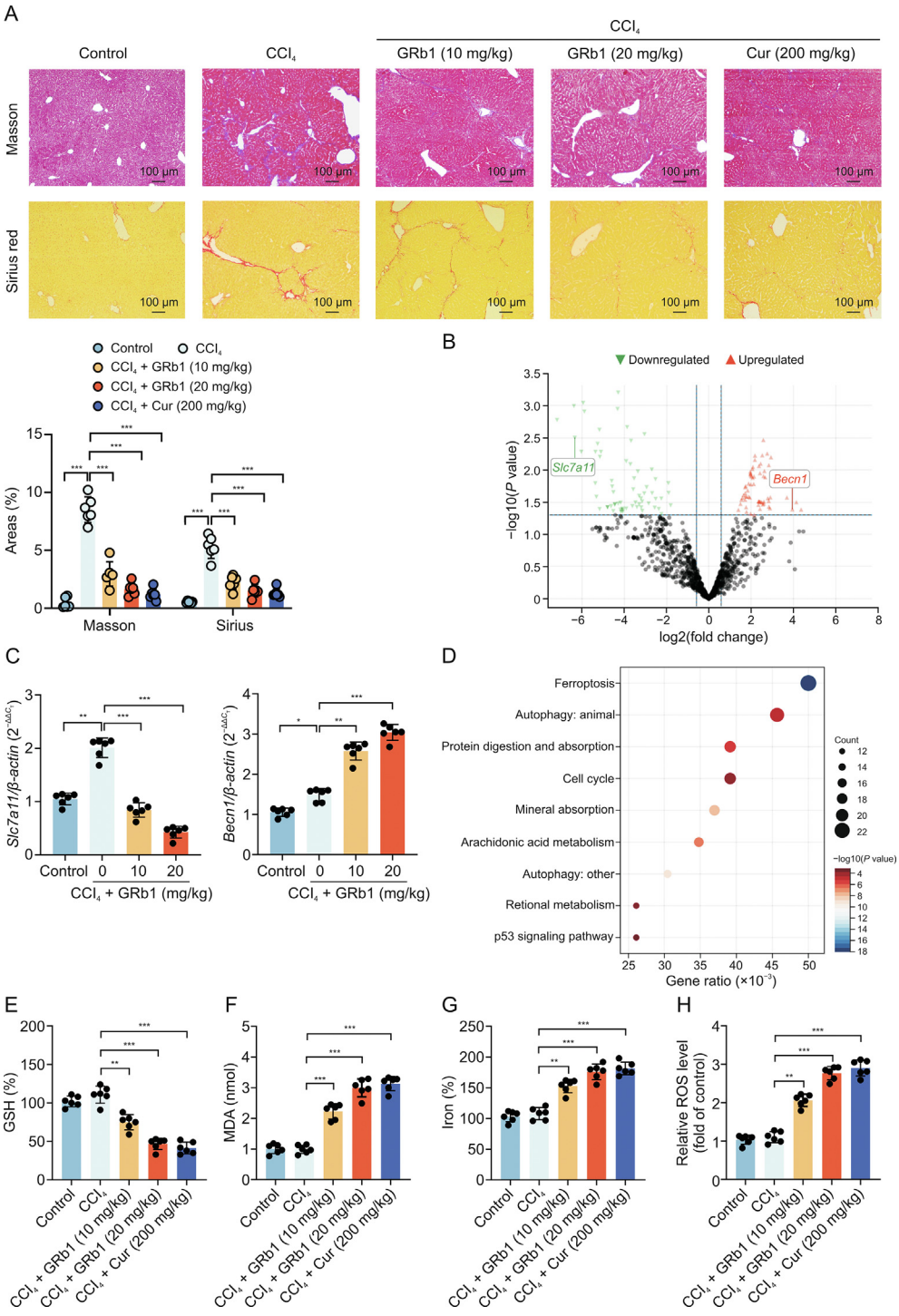

Fig. 2. Ginsenoside Rb1 (GRb1) mitigates liver fibrosis through hepatic stellate cell (HSC) ferroptosis *in vivo*. (A) Images from Masson and Sirius red stains. (B) A volcano plot displaying differentially expressed genes (DEGs) in the CCl_4 + GRb1 group when compared with the CCl_4 group. (C) Quantitative real-time reverse transcription-polymerase chain reaction (qRT-PCR) findings of *Slc7a11* and Beclin 1 (*Becn1*) in liver tissues. (D) Results from the Kyoto Encyclopedia of Genes and Genomes (KEGG) analysis. (E–H) Concentrations of glutathione (GSH) (E), malondialdehyde (MDA) (F), iron (G), and reactive oxygen species (ROS) (H) in primary HSCs from healthy mice, CCl_4-treated mice, and CCl_4-exposed mice that subsequently received either GRb1 or curcumin (Cur) treatments. $^{*}P < 0.05$, $^{**}P < 0.01$, and $^{***}P < 0.001$.

and 39% in primary HSCs in the presence of 20 μM GRb1. However, *ACSL4*, *GPX4*, and *PTGS2* levels remained relatively stable (Figs. S3A and B). Consequently, the protein expression of BECN1 and SLC7A11, uncovering an increase in BECN1 and a decrease in SLC7A11 in the GRb1-treated cells, was assessed (Figs. 5A and B). To discern the contribution of BECN1 to GRb1-triggered HSC ferroptosis, silenced *BECN1* was used. An initial validation confirmed diminished BECN1 levels in the *BECN1*-silenced cells (Fig. 5C). Intriguingly, the suppression of BECN1 countered the HSC ferroptosis instigated by GRb1. This manifested as an

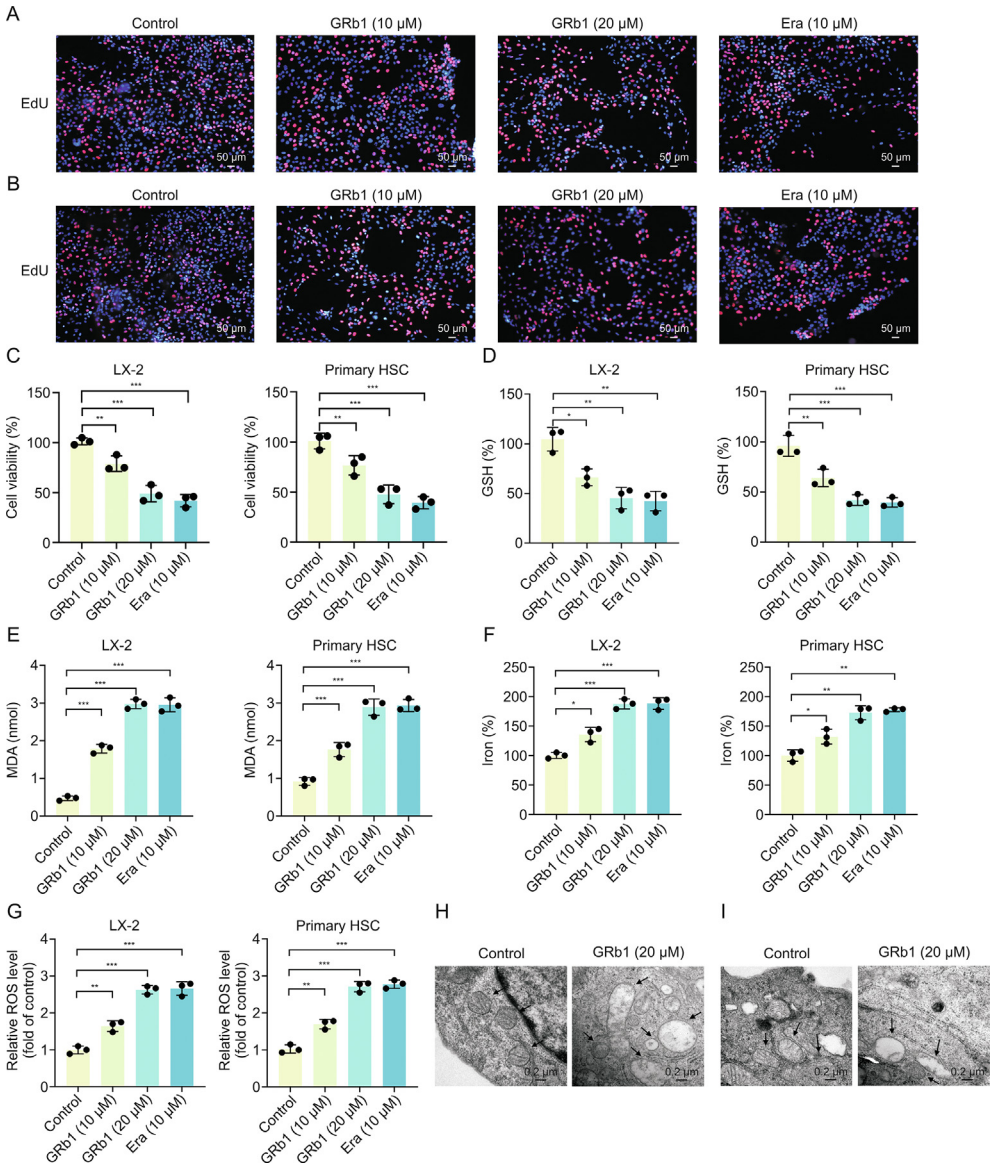

Fig. 3. Ginsenoside Rb1 (GRb1) induces hepatic stellate cell (HSC) ferroptosis *in vitro*. LX-2 cells and primary HSCs from healthy mice underwent treatment with either GRb1 (10 or 20 μM) or erastin (Era) (10 μM) for 24 h. (A, B) Results from the 5-ethynyl-2′-deoxyuridine (EdU) assay in LX-2 cells (A) and primary HSCs (B). (C) Results of the Cell Counting Kit-8 (CCK-8) assay. (D–G) Measurements of glutathione (GSH) (D), malondialdehyde (MDA) (E), iron (F), and reactive oxygen species (ROS) (G) concentrations. (H, I) Findings from the transmission electron microscopy (TEM) analysis in LX-2 cells (H) and primary HSCs (I), with arrows highlighting cell mitochondria. $^{*}P < 0.05$, $^{**}P < 0.01$, and $^{***}P < 0.001$.

elevation in cell viability (up to 77% and 80%), GSH content (up to 81% in both cases), and reductions in MDA (to 137% and 164%), iron (to 127% and 124%), and ROS levels (to 169% and 175%) in *BECN1*-silenced LX-2 cells and primary HSCs, respectively (Figs. 5D–F, S3C, and S3D). Additionally, *BECN1* knockdown upregulated α-SMA and Col1A1 concentrations in GRb1-treated cells (Figs. 5G, 5H, and S3E–H).

Furthermore, this study explored BECN1's role in the HSC activation mediated by GRb1. Using BECN1 cDNA, *BECN1* overexpression was established, with levels increasing to 292% in LX-2 cells and 295% in primary HSCs (Fig. 6A). Notably, this overexpression enhanced the ferroptosis driven by GRb1 (Figs. 6B–F). Additionally, the decline in α-SMA and Col1A1 concentrations seen in GRb1-treated cells was even more pronounced with *BECN1* overexpression (Figs. 6G–J). Collectively, these results suggest that BECN1 plays a pivotal role in GRb1-triggered HSC ferroptosis.

3.6. *Becn1* exacerbates GRb1-induced ferroptosis via SLC7A11

Considering GRb1's ability to elevate BECN1 while diminishing SLC7A11 expression, this study further probed whether BECN1 influences SLC7A11. Western blot outcomes showed that, compared with the GRb1 group, SLC7A11's expression increased to 97% upon silencing *Becn1* and dropped to 22% with *Becn1* overexpression (Figs. 7A and B). To elucidate the mechanisms underlying BECN1-mediated regulation of SLC7A11, molecular docking was performed to assess the potential interaction between BECN1 and SLC7A11. Docking results revealed a potential interaction between the two (BECN1 and SLC7A11; Fig. 7C). This interaction was corroborated by Co-IP results, which indicated a stronger interaction between BECN1 and SLC7A11 when GRb1 was present (Fig. 7D). In line with these findings, confocal immunofluorescence demonstrated substantial colocalization of BECN1 and SLC7A11 within the cytoplasm (Fig. 7E). Overall, these data propose that the

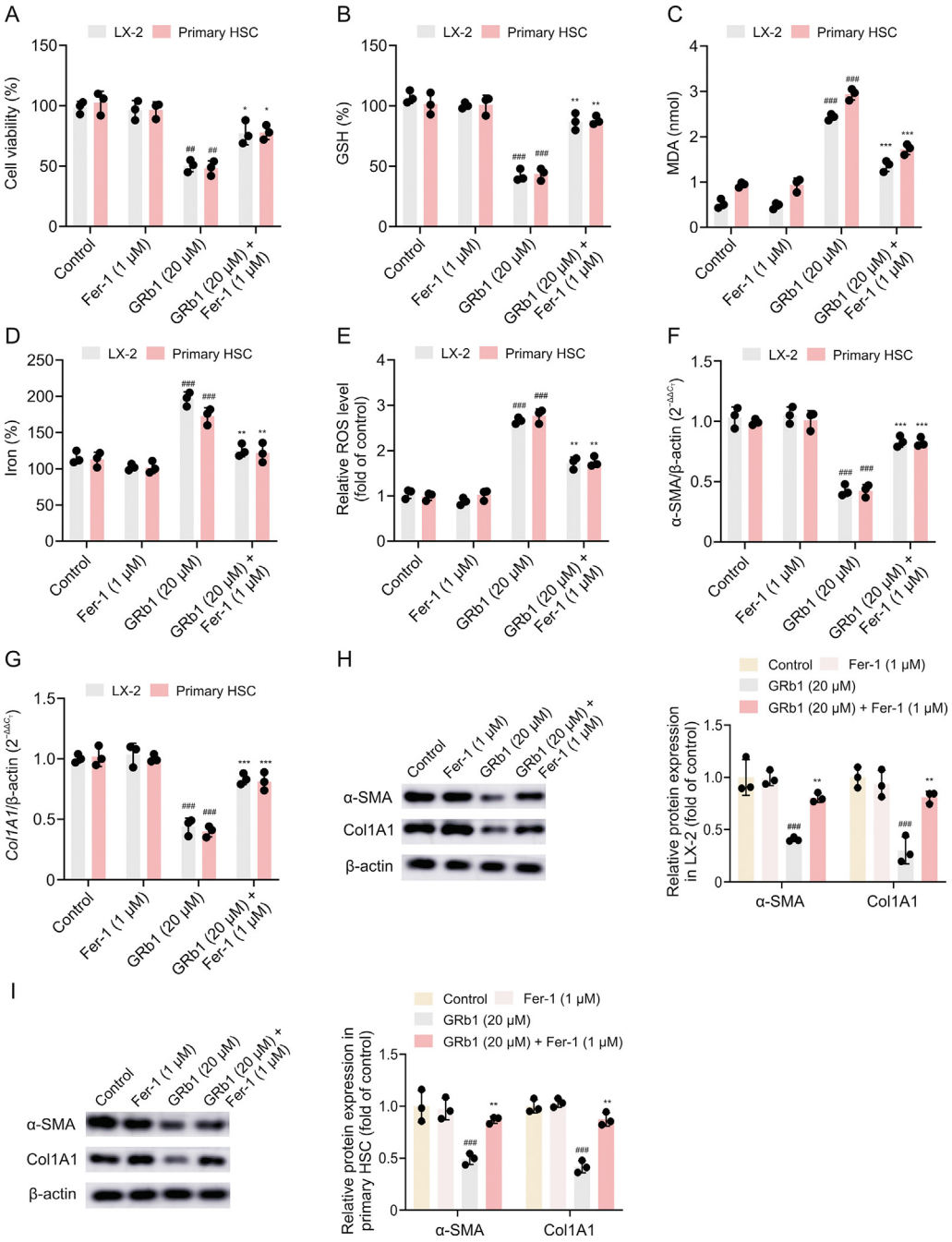

Fig. 4. Ferroptosis contributes to ginsenoside Rb1 (GRb1)'s inhibitory impact on hepatic stellate cell (HSC) activation. LX-2 cells and primary HSCs from healthy mice received treatment with GRb1 (20 μM) or ferrostatin-1 (Fer-1) (1 μM) for 24 h. Subsequently, GRb1-exposed cells underwent an additional 24 h treatment with Fer-1 (1 μM). (A) Observations from the Cell Counting Kit-8 (CCK-8) assay. (B–E) Concentrations of glutathione (GSH) (B), malondialdehyde (MDA) (C), iron (D), and reactive oxygen species (ROS) (E). (F, G) Messenger RNA (mRNA) expression levels of alpha-smooth muscle actin (*α-SMA*) (F) and type I collagen (*Col1A1*) (G). (H, I) Protein expression levels of α-SMA and Col1A1 in LX-2 cells (H) and primary HSCs (I). $^{\#\#}P < 0.01$ and $^{\#\#\#}P < 0.001$, compared to the control group. $^{*}P < 0.05$, $^{**}P < 0.01$, and $^{***}P < 0.001$, compared to the GRb1 group.

ferroptosis of HSC induced by GRb1 is mediated, at least partially, via the BECN1-SLC7A11 interaction.

3.7. Specific Becn1 knockdown in HSC impedes GRb1-induced ferroptosis in vivo

To assess whether *Becn1* knockdown can counteract the GRb1-triggered ferroptosis *in vivo*, VA-Lip-*Becn1*-shRNA was used to specifically target and suppress HSC-specific ferroptosis in CCl_4-induced mice (Fig. S4). Both Masson and Sirius staining demonstrated that *Becn1* knockdown counteracted the GRb1-driven reduction in collagen accumulation (Fig. 8A). Correspondingly, immunohistochemistry staining of α-SMA re-vealed that the GRb1-induced decrease in α-SMA was reversed with *Becn1* knockdown (Fig. 8A). After treating with GRb1 + VA-Lip-*Becn1*-shRNA, primary HSCs were isolated from the livers of CCl_4-induced mice. It was evident that *Becn1* knockdown counteracted the GRb1-driven decrease in *α-SMA* and *Col1A1* mRNA levels

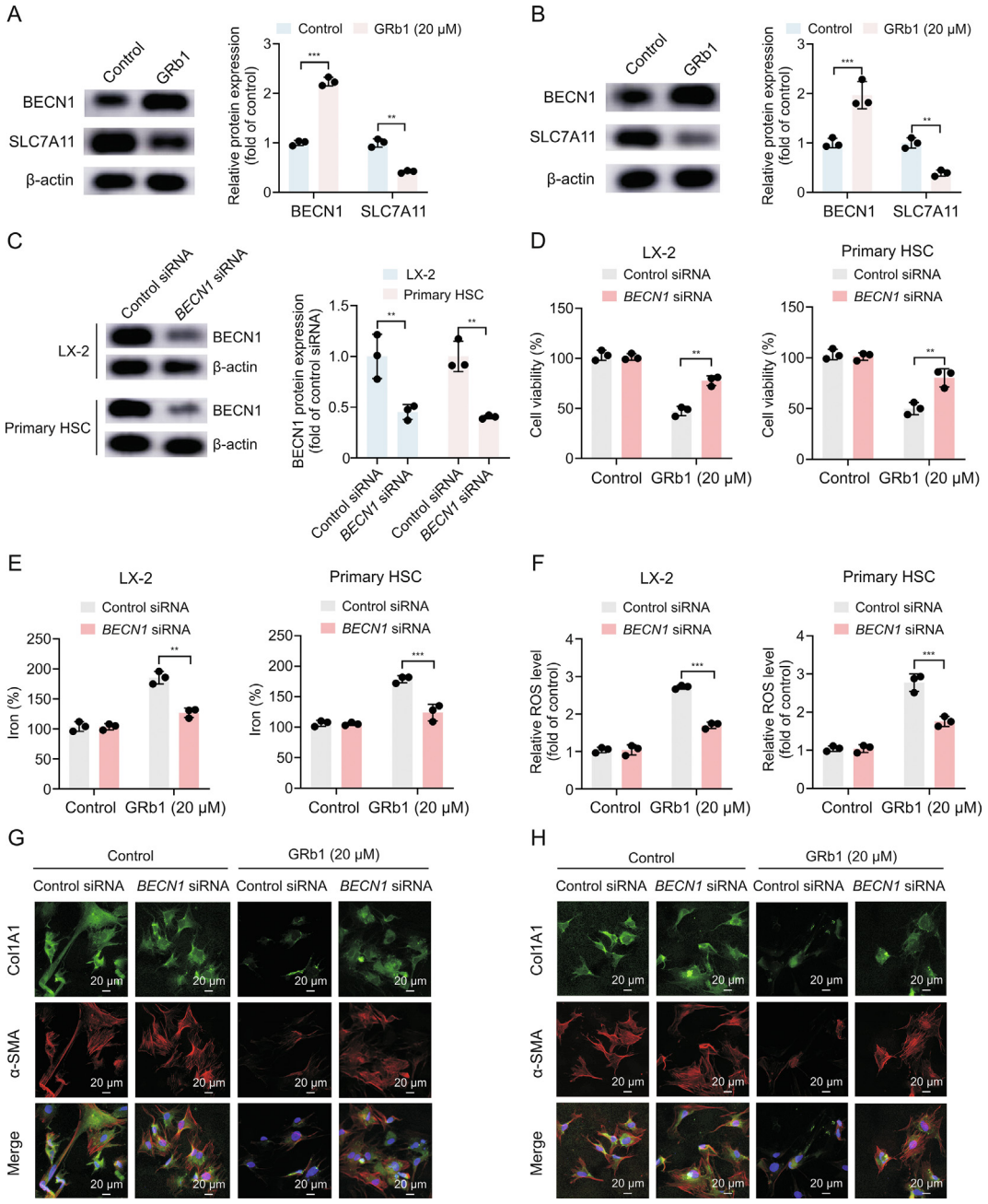

Fig. 5. Beclin 1 (*BECN1*) knockdown disrupts ginsenoside Rb1 (GRb1)-induced hepatic stellate cell (HSC) ferroptosis. LX-2 cells and primary HSCs from healthy mice received treatment with control small interfering RNA (siRNA) and *BECN1* siRNA. Following that, *BECN1*-silenced cells were exposed to GRb1 (20 μM) for 24 h. (A, B) Protein expression levels of BECN1 and SLC7A11 in LX-2 cells (A) and primary HSCs (B). (C) Protein levels of BECN1. (D–F) Measurements of cell viability (D), iron (E), and reactive oxygen species (ROS) (F) in *BECN1*-silenced cells. (G, H) Co-localizations of alpha-smooth muscle actin (α-SMA) (shown in red) and Type I collagen (Col1A1) (shown in green) in LX-2 cells (G) and primary HSCs (H) were evaluated using immunofluorescence staining. 4′,6-diamidino-2-phenylindole (DAPI) was utilized to stain nuclei in blue. $^{**}P < 0.01$ and $^{***}P < 0.001$.

(Figs. 8B and C). Additionally, the GRb1-induced increase in *Becn1* expression was nullified by *Becn1* knockdown (Fig. 8D). In contrast, *Becn1* knockdown restored the levels of GRb1-inhibited *Slc7a11* (Fig. 8E). Importantly, the GRb1-mediated increases in GSH depletion, MDA, iron, and ROS were negated by VA-Lip-BECN1-shRNA, implying that *Becn1* knockdown hinders the ferroptosis in HSCs instigated by GRb1 (Figs. 8F–I). Collectively, this evidence indicates that knocking down *Becn1* in HSCs curtails the *in vivo* ferroptosis effects of GRb1 on HSCs.

4. Discussion

The activation of HSC plays a pivotal role in the progression of liver fibrosis [22]. When the liver is injured, activated HSCs produce and accumulate ECM, resulting in significant fibrosis [23]. Inducing HSC death pharmacologically through processes such as apoptosis, ferroptosis, and senescence has proven to be an effective strategy in treating liver fibrosis [24–26]. This study identified the inhibitory effect of GRb1 on HSC activation both *in vivo* and *in vitro*. Moreover,

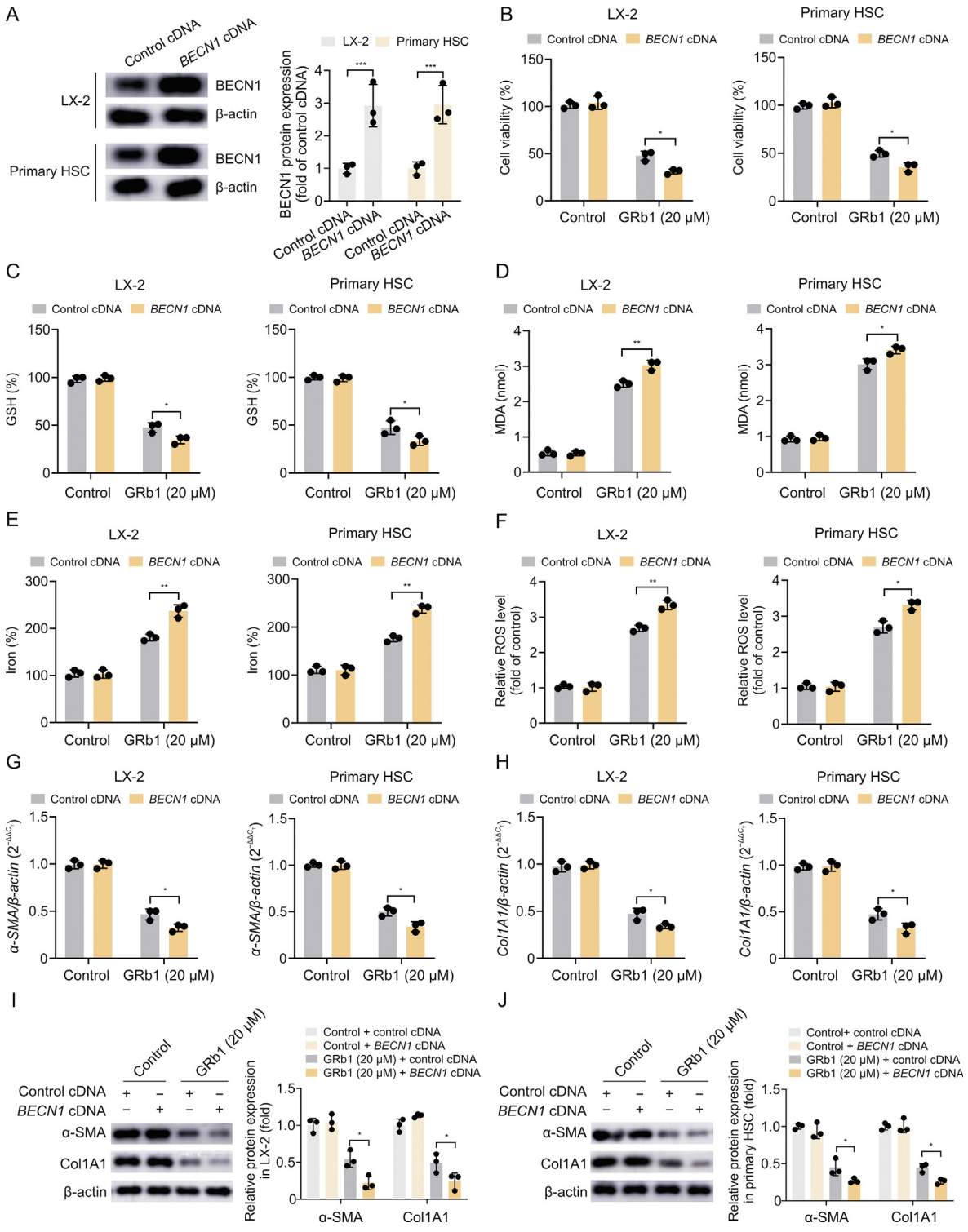

Fig. 6. Beclin 1 (*BECN1*) overexpression enhances ginsenoside Rb1 (GRb1)-induced hepatic stellate cell (HSC) ferroptosis. LX-2 cells and primary HSCs from healthy mice underwent treatment with control complementary DNA (cDNA) and *BECN1* cDNA. Subsequently, *BECN1*-overexpressing cells were exposed to GRb1 (20 μM) for 24 h. (A) BECN1 protein expression. (B–F) Cell viability (B) and levels of glutathione (GSH) (C), malondialdehyde (MDA) (D), iron (E), and reactive oxygen species (ROS) (F) in *BECN1*-overexpressing cells. (G, H) Messenger RNA (mRNA) expression levels of alpha-smooth muscle actin (*α-SMA*) (G) and type I collagen (*Col1A1*) (H) in LX-2 cells and primary HSCs. (I, J) Protein expression levels of α-SMA and Col1A1 in LX-2 cells (I) and primary HSCs (J). $^{*}P < 0.05$, $^{**}P < 0.01$, and $^{***}P < 0.001$.

the results of this study demonstrated that GRb1 contributes to promoting HSC ferroptosis and inactivation, at least in part, through the BECN1/SLC7A11 axis. This is the first report highlighting the molecular basis of GRb1-mediated ferroptosis.

GRb1, a tetracyclic triterpenoid saponin, is known for its anti-inflammatory, antioxidative, and antifibrotic properties [27–29]. For instance, Lo et al. [30] reported that GRb1 promotes the inactivation of rat HSC-T6 cells. Consistent with this, the present study

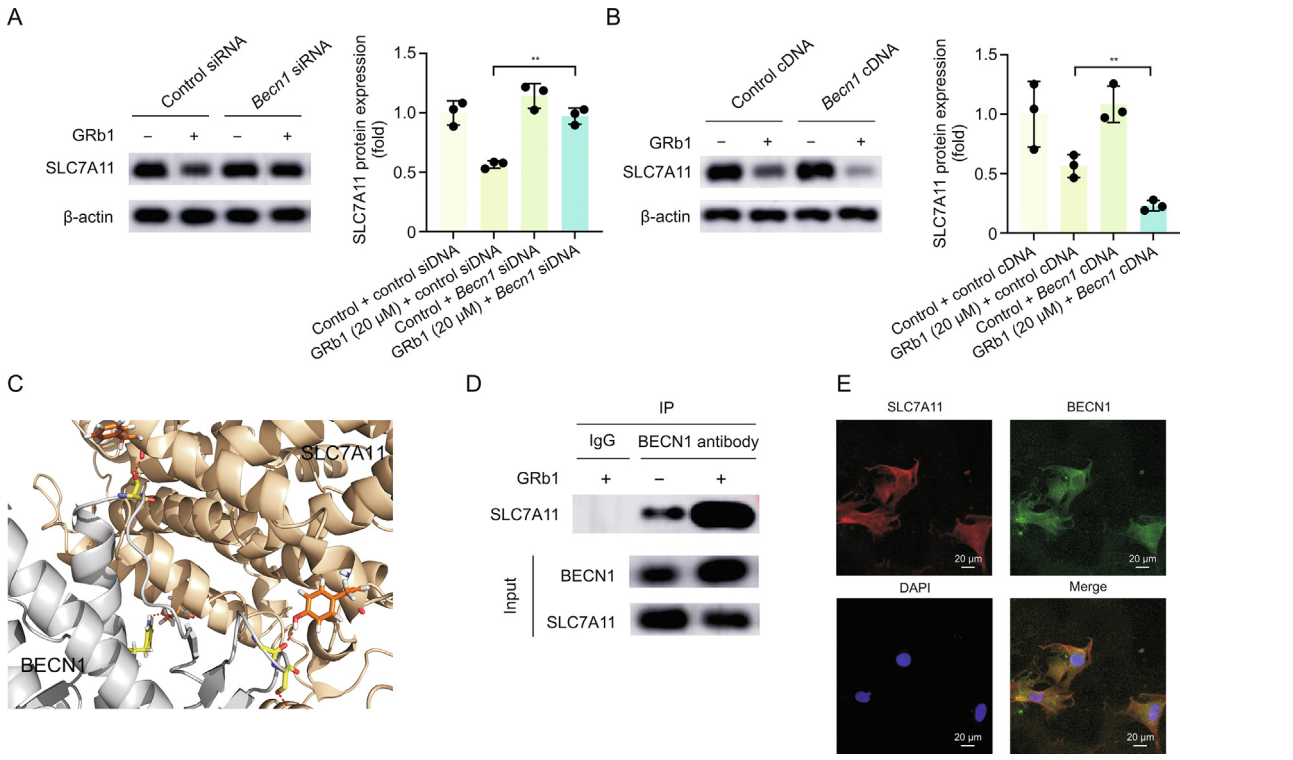

Fig. 7. Beclin 1 (BECN1) amplifies ginsenoside Rb1 (GRb1)-induced ferroptosis through SLC7A11. Primary hepatic stellate cells (HSCs) from healthy mice were treated with control small interfering RNA (siRNA), *Becn1* siRNA, control complementary DNA (cDNA), and *Becn1* cDNA. *Becn1*-silenced or overexpressing cells were then treated with GRb1 (20 μM) for 24 h. (A, B) Expression of SLC7A11 protein: *Becn1*-silenced treatment (A) and *Becn1*-overexpressing treatment (B). (C) Molecular docking analysis, with the red dotted line illustrating the interaction between BECN1 and SLC7A11. (D) Co-immunoprecipitation (Co-IP) analysis of the BECN1-SLC7A11 complex. (E) Co-localization of BECN1 (green) with SLC7A11 (red) in primary HSCs. Nuclei were stained with 4′,6-diamidino-2-phenylindole (DAPI) (blue). $^{**}P < 0.01$.

revealed that GRb1 assists in inhibiting HSC activation and mitigating liver fibrosis. Ferroptosis, a type of non-apoptotic regulatory cell death mechanism, is critical in liver fibrosis progression [31]. For example, Zhang et al. [32] revealed that the BRD7-P53-SLC25A28 axis mediates HSC ferroptosis via the mitochondrial iron metabolism pathway, thus alleviating liver fibrosis. Additionally, Wu et al. [33] found that the fibroblast growth factor 21 inhibits ferroptosis to reduce iron-induced liver damage and fibrosis. In this context, this study shows the involvement of the ferroptosis pathway in the effects of GRb1 on HSC inactivation. Upon GRb1 treatment, there was a noticeable increase in HSC ferroptosis. The ferroptosis and inactivation of HSCs, driven by GRb1, could be neutralized by Fer-1, which is a notable finding. In conclusion, GRb1 bolsters HSC inactivation, at least in part, by enhancing HSC ferroptosis.

BECN1, also referred to as ATG6, possesses multiple functions that operate independently of autophagy. These include endocytosis, cytokinesis control, cell death, and protein-protein interactions [34]. Supporting this, Hu et al. [35] showed that BECN1 has an autophagy-independent role in colorectal cancer. Furthermore, there is growing evidence linking BECN1 with ferroptosis [36]. For instance, Yin et al. [37] found that inhibiting BECN1 reduces cold stress-induced ferroptosis, while Huang et al. [38] discovered that silencing *BECN1* shields cells from ferroptosis in HCC. Recently, it was highlighted that BECN1, delivered through exosomes secreted by human umbilical cord mesenchymal stem cells, induces HSC ferroptosis by promoting the xCT/GPX4 axis [39]. In line with these findings, the data of the present study suggest that *BECN1* overexpression intensifies the effects of GRb1 on ferroptosis and HSC inactivation. *BECN1* knockdown both *in vivo* and *in vitro* effectively countered GRb1-induced HSC ferroptosis. However, the exact mechanism underlying GRb1-induced BECN1 needs deeper exploration.

SLC7A11, a critical subunit of System Xc-key, acts as an inhibitor of ferroptosis [40]. Previously, we found that ginsenoside Rh2 governs IRF1-inhibited SLC7A11, thereby promoting HSC ferroptosis and inactivation [41]. The present study showed that GRb1 promotes HSC ferroptosis by modulating BECN1-inhibited SLC7A11, leading to reduced liver fibrosis. These observations collectively hint at varied mechanisms through which different components of Panax ginseng induce HSC ferroptosis. Noteworthy, only primary HSCs were evaluated for ginsenoside Rh2's role in HSC ferroptosis. However, both primary HSCs and LX-2 cells were employed to validate the influence of GRb1 on HSC ferroptosis in this study.

Recent studies have increasingly highlighted the significance of the BECN1-SLC7A11 complex formation in the progression of human diseases. For example, Song et al. [21] found that BECN1 amplifies Era-induced ferroptosis in colon adenocarcinoma cells through its interaction with SLC7A11. Similarly, Yan et al. [42] observed that PM2.5 promotes ferroptosis by facilitating the BECN1-SLC7A11 complex in acute lung injury. In this context, the Co-IP results indicated an interaction between BECN1 and SLC7A11, which was bolstered by GRb1. This BECN1-SLC7A11 complex formation resulted in a diminished SLC7A11 level, promoting HSC ferroptosis and mitigating liver fibrosis. To the best of our knowledge, this is the first report highlighting the role of the BECN1-SLC7A11 complex in liver fibrosis and HSC ferroptosis.

While this research has made significant progress, it is not without limitations. Firstly, this study utilized only one mouse liver fibrosis model to investigate the effects of GRb1 on HSC ferroptosis.

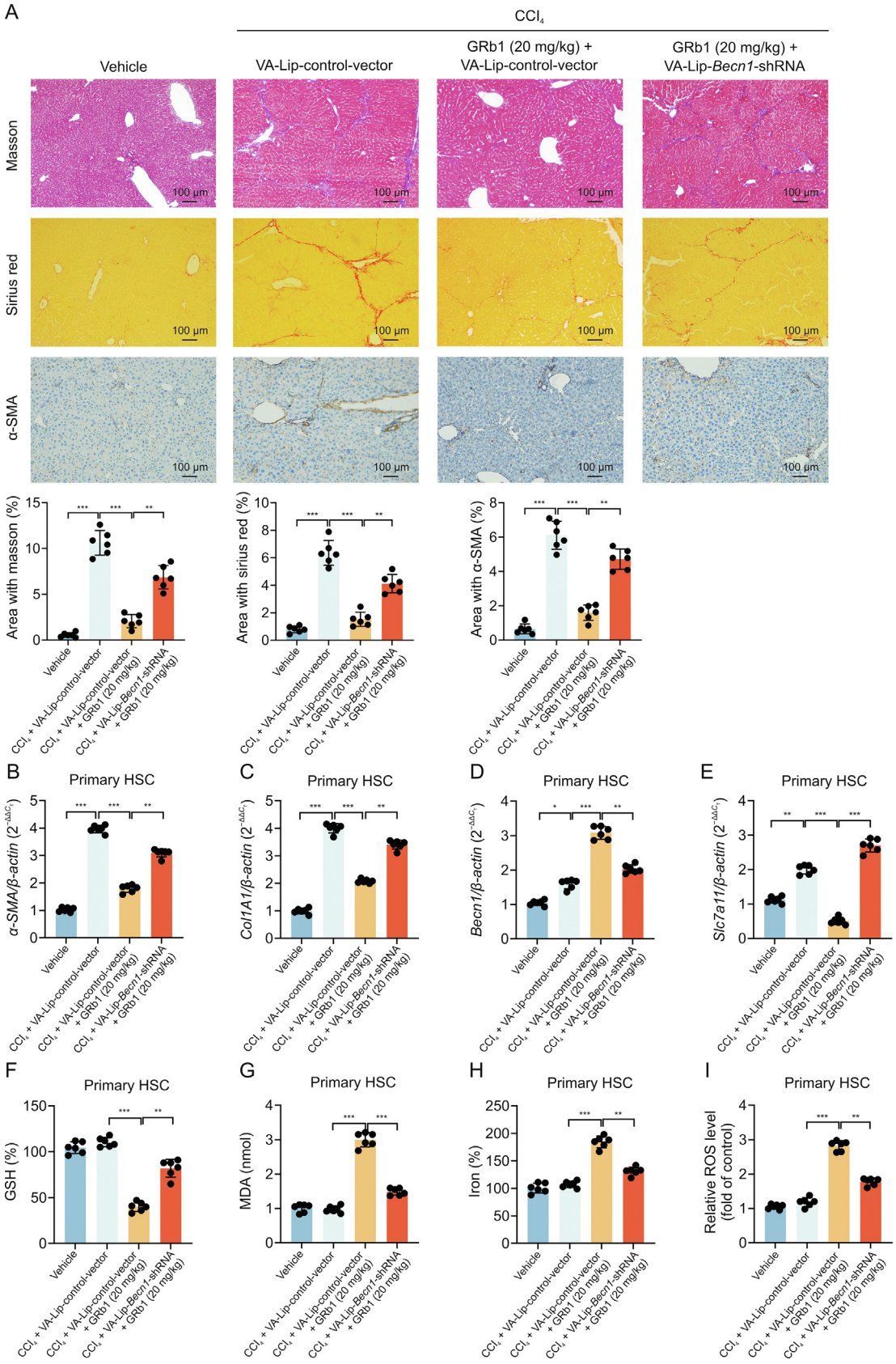

Fig. 8. Hepatic stellate cell (HSC)-specific knockdown of Beclin 1 (*Becn1*) reduces ginsenoside Rb1 (GRb1)-induced ferroptosis *in vivo*. (A) Observations from Masson, Sirius Red, and alpha-smooth muscle actin (α-SMA) immunohistochemical staining. (B–E) Messenger RNA (mRNA) expressions of *α-SMA* (B), type I collagen (*Col1A1*) (C), *Becn1* (D), and *Slc7a11* (E) in primary HSCs from vehicle-treated mice, CCl_4 + vitamin A-coupled liposomes (VA-Lip)-control-vector mice, and CCl_4-exposed mice, subsequently treated with GRb1 + VA-Lip-control-vector or GRb1 + VA-Lip-*Becn1*-short hairpin RNA (shRNA). (F–I) Levels of glutathione (GSH) (F), iron (G), malondialdehyde (MDA) (H), and reactive oxygen species (ROS) (I) in primary HSCs from vehicle mice, CCl_4 + VA-Lip-control-vector mice, and CCl_4-treated mice, following GRb1 + VA-Lip-control-vector or GRb1 + VA-Lip-*Becn1*-shRNA treatments. $^{*}P < 0.05$, $^{**}P < 0.01$, and $^{***}P < 0.001$.

Future research would benefit from examining additional liver fibrosis models. Furthermore, the mechanism underlying GRb1-induced BECN1 warrants deeper investigation.

5. Conclusion

Our study reveals that GRb1-enhanced BECN1 is directly bound to SLC7A11, which promotes HSC ferroptosis as well as HSC inactivation and finally alleviates liver fibrosis. The above results indicate the exact mechanism of GRb1 for ameliorating liver fibrosis. In conclusion, GRb1 triggers HSC ferroptosis and advances HSC inactivation, at least partially, by modulating BECN1 and SLC7A11. These findings indicate that GRb1 has the potential to be developed as a therapeutic drug for liver fibrosis.

CRediT author statement

Lifan Lin: Investigation, Methodology, Validation, Writing - Original draft preparation; **Xinmiao Li:** Conceptualization, Investigation, Validation; **Yifei Li:** Project administration, Supervision, Software; **Zhichao Lang:** Investigation, Validation, Methodology, Data curation; **Yeping Li:** Writing - Reviewing and Editing, Resources, Supervision; **Jianjian Zheng:** Funding Acquisition, Writing - Reviewing and Editing.

Declaration of competing interest

The authors declare that there are no conflicts of interest.

Acknowledgments

The project was supported by Wenzhou Municipal Science and technology Bureau, China (Grant No.: Y20220023), the Key Laboratory of Clinical Laboratory Diagnosis and Translational Research of Zhejiang Province, China (Grant No.: 2022E10022), and the Project of Wenzhou Medical University Basic Scientific Research, China (Grant No.: KYYW201904).

Appendix A. Supplementary data

Supplementary data to this article can be found online at https://doi.org/10.1016/j.jpha.2023.11.009.

References

[1] E. Devaraj, E. Perumal, R. Subramaniyan, et al., Liver fibrosis: Extracellular vesicles mediated intercellular communication in perisinusoidal space, Hepatology 76 (2022) 275–285.
[2] D. Karin, Y. Koyama, D. Brenner, et al., The characteristics of activated portal fibroblasts/myofibroblasts in liver fibrosis, Differentiation 92 (2016) 84–92.
[3] A. Jangra, A. Kothari, P. Sarma, et al., Recent advancements in antifibrotic therapies for regression of liver fibrosis, Cells 11 (2022), 1500.
[4] L. Qin, N. Liu, C.L. Bao, et al., Mesenchymal stem cells in fibrotic diseases-the two sides of the same coin, Acta Pharmacol. Sin. 44 (2023) 268–287.
[5] S.C. Koeberle, A.P. Kipp, H. Stuppner, et al., Ferroptosis-modulating small molecules for targeting drug-resistant cancer: Challenges and opportunities in manipulating redox signaling, Med. Res. Rev. 43 (2023) 614–682.
[6] B.R. Stockwell, J.P. Friedmann Angeli, H. Bayir, et al., Ferroptosis: A regulated cell death nexus linking metabolism, redox biology, and disease, Cell 171 (2017) 273–285.
[7] V. Otasevic, M. Vucetic, I. Grigorov, et al., Ferroptosis in different pathological contexts seen through the eyes of mitochondria, Oxid. Med. Cell. Longev. 2021 (2021), 5537330.
[8] F. Zeng, L. Ye, Q. Zhou, et al., Inhibiting SCD expression by IGF1R during lorlatinib therapy sensitizes melanoma to ferroptosis, Redox Biol. 61 (2023), 102653.
[9] P. Luo, D. Liu, Q. Zhang, et al., Celastrol induces ferroptosis in activated HSCs to ameliorate hepatic fibrosis via targeting peroxiredoxins and HO-1, Acta Pharm. Sin. B 12 (2022) 2300–2314.
[10] S. Huang, Y. Wang, S. Xie, et al., Isoliquiritigenin alleviates liver fibrosis through caveolin-1-mediated hepatic stellate cells ferroptosis in zebrafish and mice, Phytomedicine 101 (2022), 154117.
[11] Q. Ruan, C. Wen, G. Jin, et al., Phloretin-induced STAT3 inhibition suppresses pancreatic cancer growth and progression via enhancing Nrf2 activity, Phytomedicine 118 (2023), 154990.
[12] C. Chen, W. Gong, J. Tian, et al., Radix Paeoniae Alba attenuates Radix Bupleuri-induced hepatotoxicity by modulating gut microbiota to alleviate the inhibition of saikosaponins on glutathione synthetase, J. Pharm. Anal. 13 (2023) 640–659.
[13] W. Zha, Y. Sun, W. Gong, et al., Ginseng and ginsenosides: Therapeutic potential for sarcopenia, Biomed. Pharmacother. 156 (2022), 113876.
[14] Z. Lin, R. Xie, C. Zhong, et al., Recent progress (2015-2020) in the investigation of the pharmacological effects and mechanisms of ginsenoside Rb_1, a main active ingredient in *Panax ginseng* Meyer, J. Ginseng Res. 46 (2022) 39–53.
[15] Y. Ni, H. Deng, L. Zhou, et al., Ginsenoside Rb1 ameliorated bavachin-induced renal fibrosis via suppressing Bip/eIF2α/CHOP signaling-mediated EMT, Front. Pharmacol. 13 (2022), 872474.
[16] R. Zhang, X. Li, Y. Gao, et al., Ginsenoside Rg1 epigenetically modulates Smad7 expression in liver fibrosis via microRNA-152, J. Ginseng Res. 47 (2023) 534–542.
[17] I. Mederacke, D.H. Dapito, S. Affò, et al., High-yield and high-purity isolation of hepatic stellate cells from normal and fibrotic mouse livers, Nat. Protoc. 10 (2015) 305–315.
[18] J. Zhang, S. Chen, S. Wei, et al., CircRAPGEF5 interacts with RBFOX2 to confer ferroptosis resistance by modulating alternative splicing of TFRC in endometrial cancer, Redox Biol. 57 (2022), 102493.
[19] M. Shen, Y. Li, Y. Wang, et al., N^6-methyladenosine modification regulates ferroptosis through autophagy signaling pathway in hepatic stellate cells, Redox Biol. 47 (2021), 102151.
[20] Y.-L. Hou, Y.-H. Tsai, Y.-H. Lin, et al., Ginseng extract and ginsenoside Rb1 attenuate carbon tetrachloride-induced liver fibrosis in rats, BMC Complement. Altern. Med. 14 (2014), 415.
[21] X. Song, S. Zhu, P. Chen, et al., AMPK-mediated BECN1 phosphorylation promotes ferroptosis by directly blocking system X_c^- activity, Curr. Biol. 28 (2018) 2388–2399.e5.
[22] S. Sharma, D. Le Guillou, J.Y. Chen, Cellular stress in the pathogenesis of nonalcoholic steatohepatitis and liver fibrosis, Nat. Rev. Gastroenterol. Hepatol. 20 (2023) 662–678.
[23] Q. Pei, Q. Yi, L. Tang, Liver fibrosis resolution: From molecular mechanisms to therapeutic opportunities, Int. J. Mol. Sci. 24 (2023), 9671.
[24] Q. Zhang, P. Luo, L. Zheng, et al., 18beta-glycyrrhetinic acid induces ROS-mediated apoptosis to ameliorate hepatic fibrosis by targeting PRDX1/2 in activated HSCs, J. Pharm. Anal. 12 (2022) 570–582.
[25] S. Chen, J. Zhu, X. Zang, et al., The emerging role of ferroptosis in liver diseases, Front. Cell Dev. Biol. 9 (2021), 801365.
[26] K. Du, R. Maeso-Díaz, S.H. Oh, et al., Targeting YAP-mediated HSC death susceptibility and senescence for treatment of liver fibrosis, Hepatology 77 (2023) 1998–2015.
[27] H. Gao, N. Kang, C. Hu, et al., Ginsenoside Rb1 exerts anti-inflammatory effects *in vitro* and *in vivo* by modulating toll-like receptor 4 dimerization and NF-kB/MAPKs signaling pathways, Phytomedicine 69 (2020), 153197.
[28] N. Ni, Q. Liu, H. Ren, et al., Ginsenoside Rb1 protects rat neural progenitor cells against oxidative injury, Molecules 19 (2014) 3012–3024.
[29] J. Liu, G. Fan, N. Tao, et al., Ginsenoside Rb1 alleviates bleomycin-induced pulmonary inflammation and fibrosis by suppressing central nucleotide-binding oligomerization-, leucine-rich repeat-, and pyrin domains-containing protein three inflammasome activation and the NF-κB pathway, Drug Des. Devel. Ther. 16 (2022) 1793–1809.
[30] Y.-T. Lo, Y.-H. Tsai, S.-J. Wu, et al., Ginsenoside Rb1 inhibits cell activation and liver fibrosis in rat hepatic stellate cells, J. Med. Food 14 (2011) 1135–1143.
[31] J. Chen, X. Li, C. Ge, et al., The multifaceted role of ferroptosis in liver disease, Cell Death Differ. 29 (2022) 467–480.
[32] Z. Zhang, M. Guo, M. Shen, et al., The BRD7-P53-SLC25A28 axis regulates ferroptosis in hepatic stellate cells, Redox Biol. 36 (2020), 101619.
[33] A. Wu, B. Feng, J. Yu, et al., Fibroblast growth factor 21 attenuates iron overload-induced liver injury and fibrosis by inhibiting ferroptosis, Redox Biol. 46 (2021), 102131.
[34] E. Wirawan, S. Lippens, T. Vanden Berghe, et al., Beclin1: A role in membrane dynamics and beyond, Autophagy 8 (2012) 6–17.
[35] F. Hu, G. Li, C. Huang, et al., The autophagy-independent role of BECN1 in colorectal cancer metastasis through regulating STAT3 signaling pathway activation, Cell Death Dis. 11 (2020), 304.
[36] R. Kang, S. Zhu, H.J. Zeh, et al., BECN1 is a new driver of ferroptosis, Autophagy 14 (2018) 2173–2175.
[37] Z. Yin, G. Ding, X. Chen, et al., Beclin1 haploinsufficiency rescues low ambient temperature-induced cardiac remodeling and contractile dysfunction through inhibition of ferroptosis and mitochondrial injury, Metabolism 113 (2020), 154397.
[38] C. Huang, L. Chen, G. Chen, et al., SHP-1/STAT3-signaling-axis-regulated coupling between BECN1 and SLC7A11 contributes to sorafenib-induced

ferroptosis in hepatocellular carcinoma, Int. J. Mol. Sci. 23 (2022), 11092.
[39] Y. Tan, Y. Huang, R. Mei, et al., HucMSC-derived exosomes delivered BECN1 induces ferroptosis of hepatic stellate cells via regulating the xCT/GPX4 axis, Cell Death Dis. 13 (2022), 319.
[40] X. Chen, C. Yu, R. Kang, et al., Cellular degradation systems in ferroptosis, Cell Death Differ. 28 (2021) 1135–1148.
[41] Z. Lang, S. Yu, Y. Hu, et al., Ginsenoside Rh2 promotes hepatic stellate cell ferroptosis and inactivation via regulation of IRF1-inhibited SLC7A11, Phytomedicine 118 (2023), 154950.
[42] K. Yan, T. Hou, L. Zhu, et al., PM2.5 inhibits system X_c^- activity to induce ferroptosis by activating the AMPK-Beclin1 pathway in acute lung injury, Ecotoxicol. Environ. Saf. 245 (2022), 114083.